이학석사학위논문

Impact of Initialization on Ensemble Prediction of Intraseasonal Oscillation during Boreal Summer

북반구 여름철 ISO 앙상블 예측에 대해 초기화 과정이 미치는 영향

2013 년 2 월

서울대학교 대학원

지구환경과학부

장 평 화

Abstract

Impact of Initialization on Ensemble Prediction of Intraseasonal Oscillation during Boreal Summer

Pyong-Hwa Jang

School of Earth and Environmental Sciences

The Graduate School

Seoul National University

The Impact of initialization and perturbation methods on the ensemble prediction of the boreal summer intraseasonal oscillation was investigated with the 20-year hindcast predictions from a coupled general circulation model (CGCM). The three perturbation methods used in the present study included the lagged averaged forecast (LAF), the Breeding, and the empirical singular vector (ESV)

methods. The hindcast experiments were performed with a prediction interval of every 10 days for an extended boreal summer (May- October) season over a 20-year period.

The empirical orthogonal function (EOF) eigenvectors of the initial perturbations depended on the individual perturbation methods. The leading EOF eigenvectors of the LAF perturbations exhibited large variances in the extratropics. The Bred vectors with a breeding interval of three days represented a local unstable mode moving northward and eastward over the Indian and western Pacific region, and the leading EOF modes of the ESV perturbations represented the planetary-scale eastward moving perturbations over the tropics. By combing the three perturbation methods, a multi-perturbation (MP) ensemble prediction system for the intraseasonal time scale was constructed, and the effectiveness of the MP prediction system for the Madden and Julian Oscillation (MJO) prediction was examined in the present study. The MJO prediction skills of individual perturbation methods were all

similar, however, the MP-based predictions had a higher correlation skill in predicting the real-time multivariate Madden-Julian Oscillation (RMM) indices compared to those of the individual perturbation methods. The predictability of the intraseasonal oscillation is sensitive to the MJO amplitude and to the location of the dominant convective anomaly at the initial state. The improvement in skill of the MP prediction system was more effective during periods of weak MJO activity.

Keywords

Multi-Perturbation ensemble prediction system, Perturbation method, Boreal summer intraseasonal oscillation, Madden-Julian Oscillation, Predictability

Student number : 2011-20378

Contents

Table and Figure Captions

You can see the original figures and table at

http://m.site.naver.com/04MtY or here :

1. Introduction

A number of studies have examined and predicted the intraseasonal oscillation (ISO)/Madden-Julian Oscillation (MJO), by recognition of its influence on the variability of the climate and the weather (Kessler 2001; Wheeler and McBride 2005; Hoyos and Webster 2007). Several statistical models have been utilized to predict intraseasonal variability, whereas predictions with dynamical models have been limited until recent years, mainly due to poor ISO simulations (Waliser et al. 1999; Webster and Hoyos 2004; Jiang et al. 2008). However, recent dynamical models have improved in their ability to simulate the MJO, especially by improving their convection schemes and air-sea interaction factors (Wang and Schlesinger 1999; Maloney and Hartmann 2001; Vitart et al. 2007; Lin et al. 2008). As a result, current dynamical forecasts are shown to be superior to statistical forecasts in predicting the MJO (Seo et al. 2005; Kang and Kim 2010). Recently, several studies have emphasized optimal initialization methods for a further improvement of the MJO

prediction skill, especially at the beginning of the forecast (Vitart et al. 2007; Ham et al. 2012a). However, systematic examinations of various initialization and perturbation methods for MJO predictions have not been sufficiently carried out at present.

Various initial perturbation methods involving the use of the ensemble prediction system have been developed and their impacts on the prediction skill have been examined with different prediction models (Palmer et al. 1994; Liess et al. 2005; Vitart et al. 2007; Yang et al. 2008; Ham et al. 2009, 2012a,b; Rashid et al. 2011; Kug et al. 2010, 2011; Ham and Kang 2010; Rashid et al. 2011). Among them are the lagged-average forecast (Rashid et al. 2011), the breeding (Yang et al. 2008, 2009; Ham et al. 2012b), the singular vector (Molteni and Palmer, 1993; Palmer et al. 1994), and the empirical singular vector methods (Kug et al. 2010, 2011; Ham and Kang 2010; Ham et al. 2012a) Most of those studies are either for weather forecasts or for the seasonal predictions, while a few studies are for intraseasonal predictions (Mureau et al. 1993; Molteni et al. 1996; Xue et al. 1997a,b; Cai et al. 2003; Vitart et al. 2007; Yang et al. 2008; Wei et al. 2008; Kug et al. 2009; Ham et al. 2009;

Vitart and Molteni 2010). In particular, Chikamoto et al. (2007) used the breeding method to isolate unstable modes associated with intraseasonal variability. Specifically, they extracted the most suitable bred vectors representing the unstable MJO mode by examining the properties of breeding perturbations associated with various rescaling factors. However, long-term prediction experiments with the breeding method were not conducted. Therefore, the impact of breeding perturbation on MJO predictions was not assessed. Ham et al. (2012) demonstrated that optimal perturbations obtained based on the empirical singular vectors produce a higher level of correlation skill when predicting the MJO compared to those using random perturbations. While previous studies focused on each individual perturbation method for MJO predictions, examinations and comparisons of various perturbation methods with the same prediction system have not been systematically carried out, particularly for ensemble MJO predictions.

It was also found that the individual perturbation methods produce different initial perturbations. Magnusson et al (2008)

compared the performances of seasonal ensemble predictions with the initial perturbation methods produced by the singular vector (SV) and the breeding (BD) methods. They concluded that the SV method offers slightly better performance globally, but that the BD method performs better in the tropics, indicating that the two methods capture different unstable modes. The ensemble prediction, outperforming individual single predictions, is made based on slightly different initial conditions (Shukla et al. 1994, 2000; Molteni et al. 1996; Buizza et al. 2000, 2007; Kang and Yoo 2006). It is expected that ensemble MJO predictions based on various initial perturbations made by various perturbation methods may produce a higher level of prediction skill compared to that with an individual perturbation method. The present study is also motivated by the possible improvement of the MJO prediction skill by combining various perturbation methods.

The ISO during boreal summer exhibits eastward as well as distinctive northward propagations over the Indian Ocean and the Asian monsoon region, while the ISO during the boreal winter shows predominantly eastward propagation. The ISO has a more complex

structure during boreal summer compared to the boreal winter ISO. Therefore the predictability of the boreal summer ISO is limited comparable to that of the boreal winter ISO (Waliser et al. 2003a, b; Ding et al. 2011). Most previous studies related to ISO predictions have focused on the boreal winter MJO while less attentions has been paid to MJO predictions during the boreal summer, despite the fact that summer predictions have much room for improvement (Slingo et al. 1999; Lo and Hendon 2000; Sperber and Waliser 2008; Ding et al. 2010; Kang and Kim 2010; Ham et al. 2012a).

The purpose of this study is to examine three perturbation methods, the LAF, the BD, and the ESV methods, systematically with the same coupled GCM and to compare the ISO prediction skills levels during boreal summer as obtained with the individual perturbation methods. Another objective is to develop a multi-perturbation (MP) ensemble MJO prediction system to assess the effectiveness of the skill improvement of the MP prediction system compared to those of individual perturbation methods. Section 2 introduces the model used in the present study. Section 3 describes the ensemble perturbation

methods adopted and examines the characteristics of the initial perturbations produced by the individual perturbation methods. The various prediction experiments with the three perturbation methods and the MP prediction system are described and their prediction skill levels are shown in Section 4. A brief summary and a discussion are presented in Section 5.

2. The Model

The model used in the present study is the Seoul National University coupled general circulation model (SNU CGCM, Kim et al. 2008; Ham et al. 2012c). The atmospheric part of the coupled model (SNU AGCM) has a spectral truncation at T42 and has 20 vertical sigma levels. Several studies have attempted to simulate the MJO realistically with the present model (Lee et al. 2001; Lin et al. 2008; Frierson et al. 2010; Kim et al. 2011). A triggering mechanism in the convection schemes plays an essential role in simulating the MJO

realistically. The Tokioka modification (Tokioka et al. 1988) is required for better simulation of the MJO with a simplified version of the Relaxed Arakawa-Schubert scheme (RAS, Moorthi and Suarez 1992), which is adopted as a convection scheme in the present model. The value of the Tokioka parameter (α), which controls the intensity of deep convection, is set to 0.1 in the present model. Another parameter affecting the MJO simulation was found to be the e-folding time scale of the auto-conversion precipitation process. The present model uses 3,200 seconds for the auto-conversion time scale. The ocean part of the coupled model is version 2.2 of the Modular Ocean Model (MOM, Pacanowski 1996) developed at the Geophysical Fluid Dynamics Laboratory (GFDL). There are 32 vertical levels with 23 levels in the upper 450 m. The top 10 layers are divided by a constant thickness of 10 m. The zonal grid spacing is 1.0°. The meridional grid spacing between 8°S and 8°N is (1/3)°, gradually increasing to 3.0° at 30°S and 30°N, and it is fixed at 3.0° poleward. The coupled model exchanges SST, wind stress, freshwater flux, longwave and shortwave radiations, as well as turbulent heat fluxes once every two hours. No flux

correction is applied, and the coupled model does not exhibit significant climate drift during free integrations. The details of the coupled model can be found in Ham et al. (2012c).

Free integration was performed for 20 years with the SNU CGCM. The ISO component was extracted by applying a 20-100 day band-pass filter to the model simulated data and observation data. The observed wind fields used are from the European Centre for Medium-Range Weather Forecasts (ECMWF) reanalysis interim data (ERA-interim, Simmons et al. 2007; Uppala et al. 2008). Figure 1 displays the phase composites of the filtered 200-hPa velocity potential anomalies of the model along with the observed values. The composites were constructed for each of the eight phases of the Wheeler-Hendon MJO index (Wheeler and Hendon 2004). The findings show that upper-level divergence over the Indian Ocean slowly moves eastward and re-enters the Indian Ocean to complete a full cycle. The simulated upper-level divergence anomalies associated with all phases of the MJO mimic the observed counterparts reasonably well, although the simulated amplitude is slightly weaker than the observed case near the

Maritime continent.

Figure 2 shows the spatial structures of the combined empirical orthogonal function (EOF) modes of three 20–100-day filtered variables of the 850-hPa and 200-hPa zonal winds and the outgoing longwave radiation (OLR), averaged meridionally for 15°S–15°N. The first mode of observational data captures the enhanced convective activity over the Indian Ocean and the Maritime continent, while the second mode captures the enhanced convection over the western and central Pacific Ocean (Figure 2a). The time series associated with the first two modes (not shown) have a quadrature relationship, indicating that the two modes are associated with an eastward propagating MJO mode. The upper- and lower-level zonal winds are clearly out of phase as regards each other, showing a baroclinic structure of the MJO. The model captures the observed characteristics of the MJO mentioned above reasonably well, although the OLR anomalies are weaker than the observed values. It should be noted that while the model captures the wind anomalies associated with the MJO reasonably well, the MJO precipitation anomalies are somewhat weaker than the observed

values in the free run.

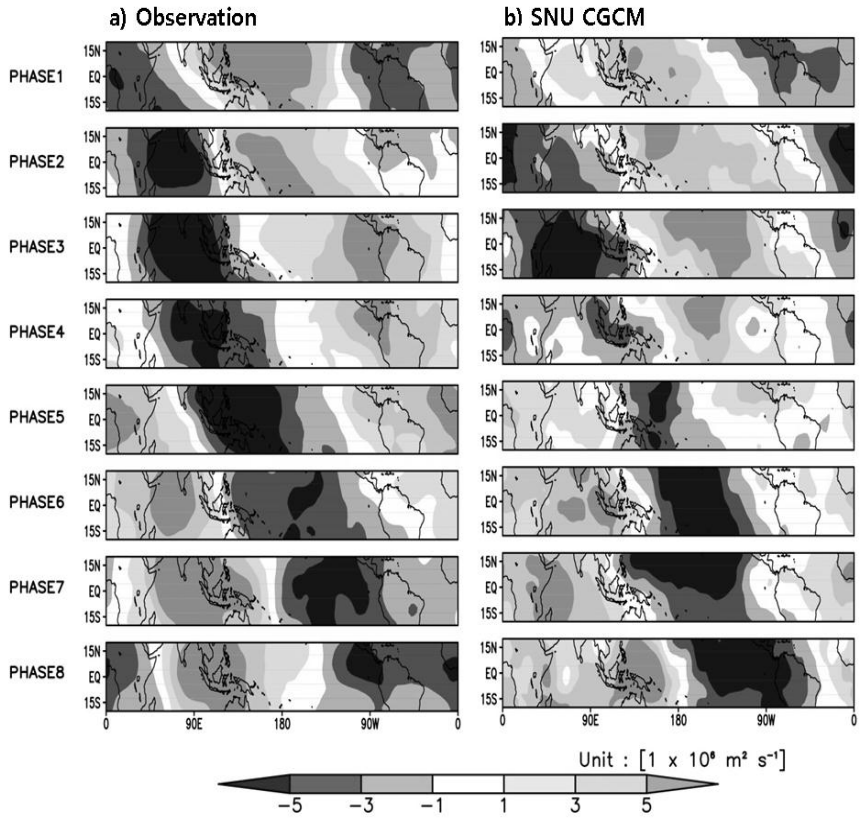

Figure 1. Phase composites of velocity potential at 200 hPa for a) observation and b) SNUCGCM. Units are $m^2\ s^{-1}$.

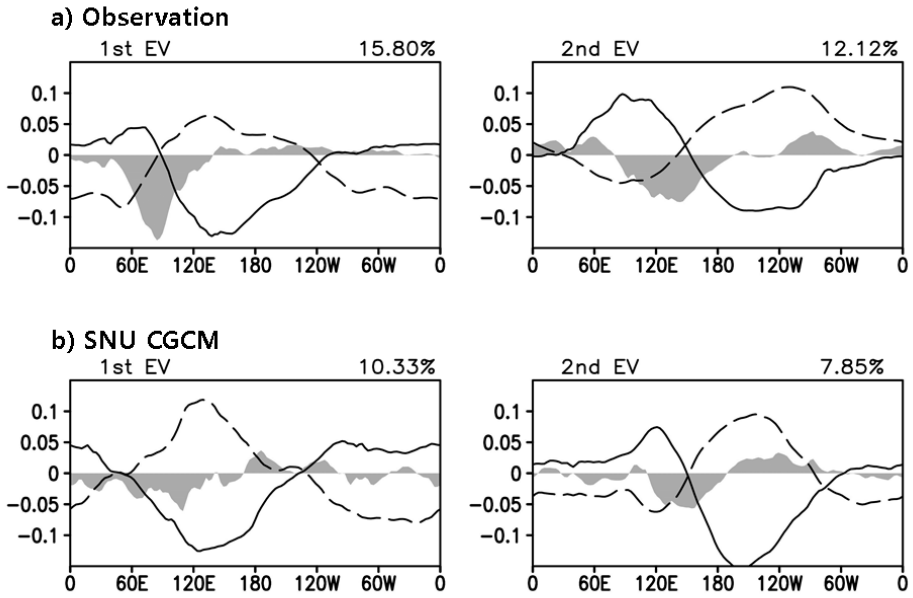

Figure 2. Two leading eigenvectors of the combined EOF of the 20-100 day filtered OLR (shaded) and zonal wind fields at 200 hPa (dashed line) and 850 hPa (solid line), meridionally averaged between 15°S and 15°N: (a) the observational data used are the ERA interim data for the wind fields and the AVHRR data for the OLR, and (b) SNUCGCM. The percentage variance explained by each mode is shown in the upper right corner of each panel.

3. Initialization and ensemble perturbation method

The initialization method adopted is the nudging method, which forces the model solution toward the observed results. For the ocean, the temperature and salinity obtained from the Global Ocean Data Assimilation System (GODAS; Behringer and Xue 2004) reanalysis are nudged from the surface to a depth of 500m with a five-day relaxation time scale. For the atmosphere, the zonal and meridional winds, temperature, surface pressure and moisture fields obtained from the ERA-interim analysis are nudged for all vertical levels with a six-hour relaxation time scale. To obtain the initial conditions, the coupled GCM was integrated with the nudging process for the entire prediction period starting on 1 January 1979. The nudging-processes are able to track the model states toward the observed states (Figure 3).

The three perturbation methods, in this case the Lagged-Averaged Forecast (LAF), Breeding (BD), and Empirical Singular Vector (ESV) methods, are employed to produce initial perturbations, which will be

added in the initial condition for the ensemble predictions (Figure 4). The LAF method utilizes nudged data at several different time lags as the initial conditions. The interval of the time lag adapted here is six hours. Four LAF initial conditions are used in the present study with time lags from 0 hr to 18 hrs for a LAF ensemble prediction. An increase in the ensemble size with the LAF method does not contribute the skill improvement of the prediction for a few weeks, as a longer lag results in a large bias of the initial condition. The average of the four ensemble predictions is defined as the LAF prediction. To identify the characteristics of the LAF perturbations, the EOF analysis is applied to all of the perturbations for the prediction period. The LAF perturbations are obtained by the difference between the nudged data at an initial time and the same data but with a time lag from the initial time. The leading two EOF eigenvectors shown in Figure 5 indicate that the LAF perturbations have a large amplitude over extratropics but are relatively small in the tropics, given that the large-scale perturbations associated with time lags of less than one day result mainly from synoptic disturbances in the extratropics.

The second perturbation method used in this study is the breeding method, as described by Toth and Kalnay (1993, 1997). The bred perturbations are realized by rescaling down the difference between a control run and a perturbation run with a certain breeding interval. The norm is used as reference in the rescaling. This is defined here as the area-averaged root mean square (RMS) of 850-hPa zonal wind for the domain of 20°S - 30°N and 40°E - 180°E. The rescaling factor adopted in this study is 10%, which was determined after examining various rescaling factors, in this case 0.3%, 3%, and 10%. It is important to note that the rescaling factors of 0.3% and 3% produced large growth rates, which appear to be related to the convective and synoptic instability. A similar result was obtained by Chikamoto et al. (2007). The bred perturbations with a rescaling factor of 10% display large amplitude variations over the Indian Ocean and the western Pacific, where tropical ISO activity is dominant (not shown). The breeding interval (window) was selected after examining the breeding perturbations produced with the intervals of one day, three days and five days with a rescaling factor of 10 %. The five-day interval

produces the bred perturbations, whose amplitudes are too weak, and their maximum variance appears on the East Pacific region. The one-day interval produces small-scale unstable modes. In contrast, the three-day interval produces perturbations, similar to the ISO patterns appearing during the boreal summer. Figure 5b shows two leading EOF eigenvectors of the BD perturbations produced with the three-day window and the 10% rescaling factor. The spatial patterns of the eigenvectors are similar to those associated with the boreal summer ISO. The associated time series have a quadrature relationship (not shown), indicating that the two patterns represent the perturbations moving northward from the Indian Ocean to the Indian subcontinent and eastward from the Indian Ocean to the western Pacific.

The ESV method used in this study follows the procedure described in Kug et al. (2010). The PC time series used in the ESV are obtained from the extended EOF analysis of the 15°S–15°N averaged 850 hPa and 200 hPa zonal winds and 200-hPa velocity potential. The ESV data in the initial state are the PC time series at the initial conditions and those at the final state utilize the PC time series obtained from the

hindcast data at a specific lead time of the prediction. 20-year hindcast data was generated in advance using the LAF method. As noted in previous studies, the ESV depends on the number of PC time series used and on the lead time of the final state. Here, we use five PC time series for both the initial and final states and a ten-day lead time, as this case produces a leading unstable mode separated distinctively from the four other damped modes. This unstable mode is defined as a leading singular vector. Adding more PC time series captures the small-scale extratropical unstable modes. The ESV initial perturbations are generated by the linear regression of the singular time series of the initial state to all of the variables. Figure 5c shows two leading EOF eigenvectors of ESV perturbations, whose spatial patterns are represented by a planetary scale of zonal wave number 1 over the tropics. It is important to note that the BD method produces relatively large perturbations that are confined to the Indian and western Pacific region, whereas the ESV method produces planetary-scale perturbations that zonally propagate across the tropical belt.

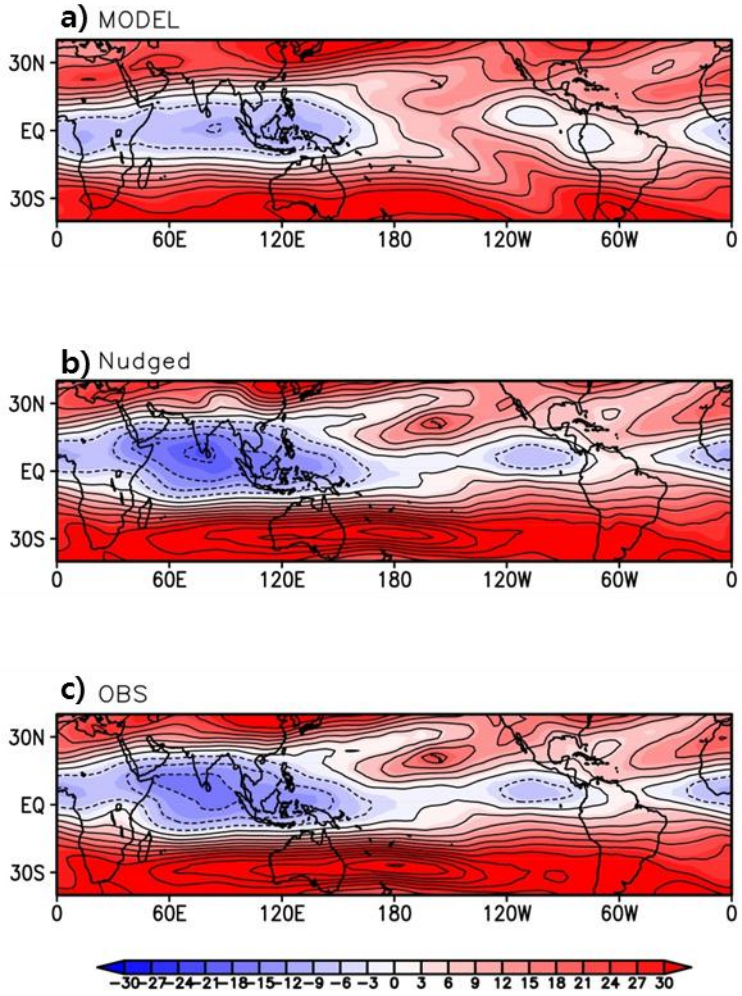

Figure 3. Time-mean (climatological) map of 200-hPa zonal wind (m s^{-1}) for a) ERA interim, b) SNU CGCM, and c) Nudged data. All data are calculated during May-October in 20 years.

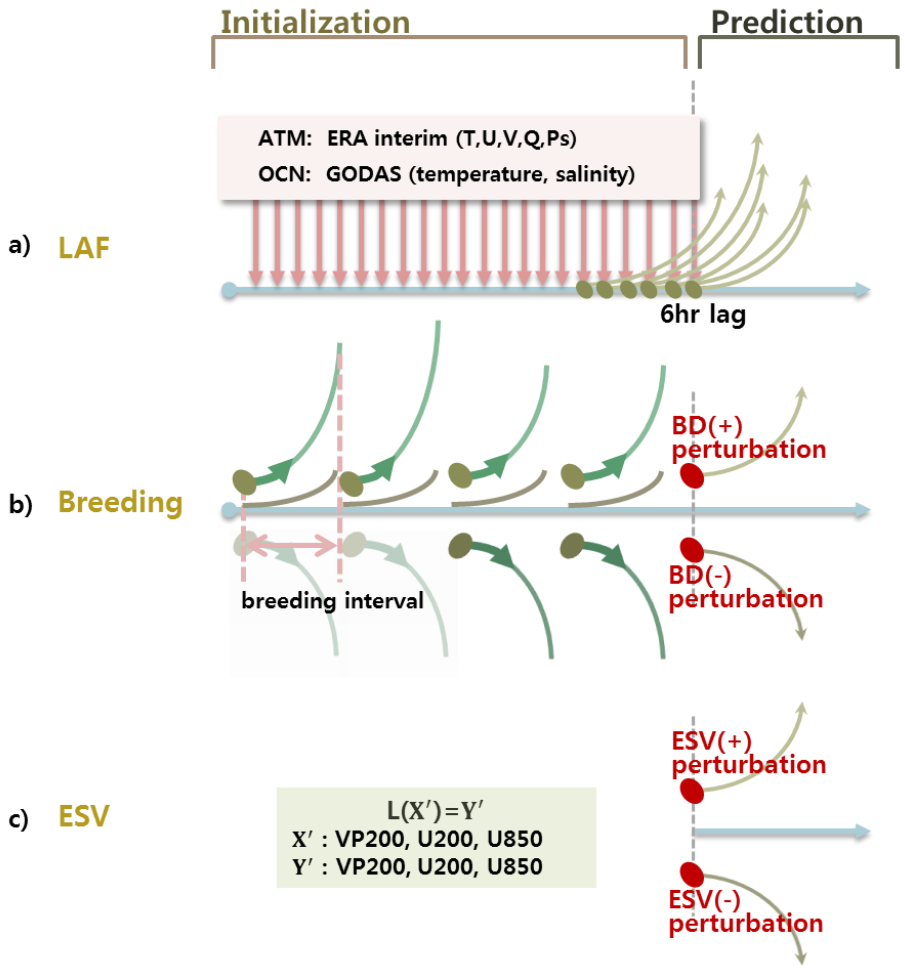

Figure 4. Schematic diagram illustrating three kinds of initialization method to generate perturbations.

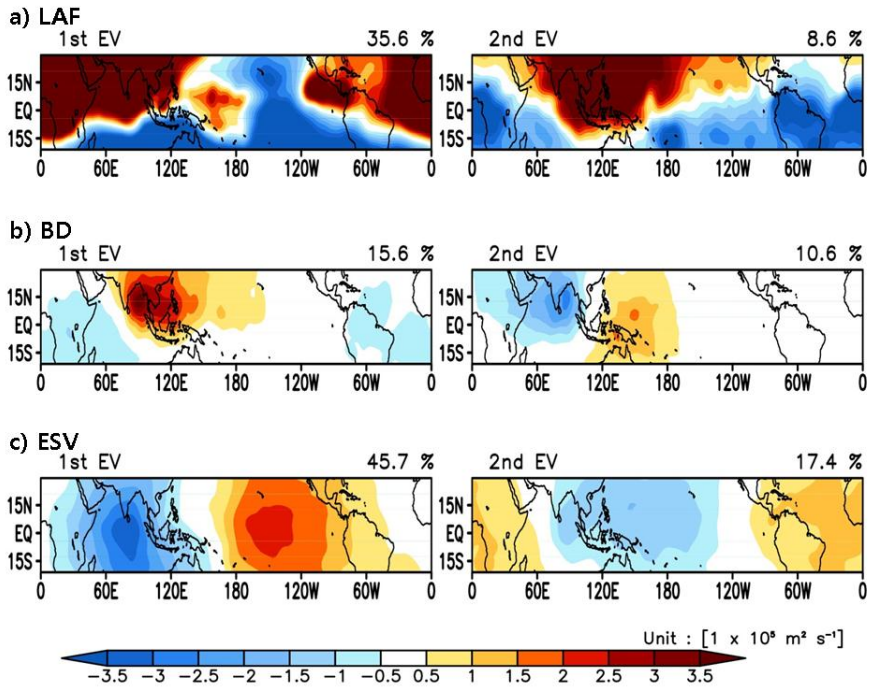

Figure 5. The first two EOF eigenvectors of the initial perturbations of the velocity potential at 200 hPa, obtained from a) the LAF, b) the Breeding, and c) the ESV methods. The percentage variance explained by each mode is shown in the upper right corner of each panel. Units are 10^5 m^2 s^{-1}.

4. Prediction experiments and MJO predictability

The serial run experiments were performed for the 20 summers of 1989–2008 (Figure 6). In this experiment, a model prediction was made for the first, eleventh and twenty-first days from May to October and each prediction lasted for 45 days. The serial integration approach has proven useful in assessing the forecast skill because it covers mostly all convective stages of the MJO. All the predictions here were assessed as the real-time multivariate Madden–Julian oscillation (RMM) indices. The RMM indices are the time series related with the first (RMM1) and second (RMM2) eigenvectors of the combined EOF of the OLR and zonal wind fields at 200 and 850 hPa over the tropical belt, averaged between 15°S and 15°N removing the interannual variability. The anomaly related to the MJO is calculated by subtracting the seasonal cycle and the previous 120-day mean, in order to remove the interannual variability (Wheeler and Hendon 2004).

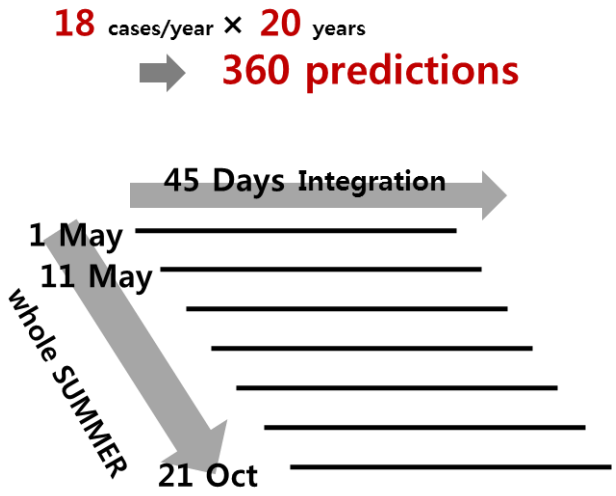

Figure 6. Schematic diagram of the serial integrations. Each experiment consists of a series of 45-day forecasts that are initialized every 10 days on 1st, 11th, and 21st of each calendar month during the entire 20-year period. For example, a single forecast run starts on 1 May 2000 and progresses for 45 days. The forecast is repeated starting on 11 May 2000 for a further 45-day forecast. This procedure is repeated for the entire years (1989-2008).

4.1. Individual perturbation ensemble prediction systems

The boreal summer MJO predictabilities of the individual perturbation methods were assessed based on the correlation of the RMM indices between the observation and the prediction. In the present study, the correlation skills of RMM1 and RMM2 are combined into one correlation skill by averaging them, and the average skill is referred to as the correlation skill of the RMM index. Figure 7 shows the RMM correlation skills of the individual perturbation methods. Interestingly, all of the methods produce similar prediction skills. The period of the MJO prediction limit exceeds 22 days, when the limit is defined with a correlation skill of 0.5 (Kang and Kim 2009). It was also noted that when the correlation skills are examined for individual variables separately instead of with the RMM index, the BD and ESV prediction skills are somewhat higher than that of the LAF for the wind variables but are similar for the OLR field (not shown).

The ensemble spread is an important property of ensemble predictions for determining the probabilistic forecast (Palmer et al. 2004). Figure 8 shows the ensemble spreads of the 200-hPa zonal wind averaged over the tropics between 15°S and 15°N for the forecast lead times from the initial time to day 30. The computed ensemble spread is defined here as the root mean square of the deviations of ensemble members from the ensemble mean. At the initial time, the LAF spread is much larger than those of the BD and ESV methods. On the other hand, the initial ESV perturbations are very small compared to those of other methods. However, the spreads grow exponentially until day 15 to 20 and are mostly saturated after approximately day 20 for all perturbation methods. It was also noted that the magnitudes of the saturated spreads are similar for all the methods. These results indicate that the ensemble spread for the ESV method grows much faster than those of the other methods, particularly compared to the LAF method. This result is due to the fact that the unstable modes reside in the initial perturbations of the ESV and in the BD perturbations. The ESV method produces planetary-scale perturbations, which have faster

growth rate compared to those of the BD perturbations. It was also noted that when all ensemble members created by the three methods are used, the ensemble spread value is between the values of the LAF and ESV methods for shorter lead times before day 15, whereas they can increase slightly (most likely remaining virtually identical, however) after the saturation of the spread.

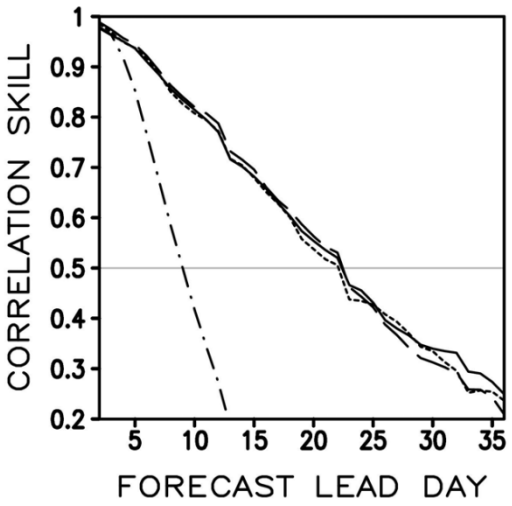

Figure 7. Correlation skill for the RMM index of the LAF (solid line), the BD (dashed line), and the ESV (dotted line). The dot-dashed line indicates the performance of a persistence forecast.

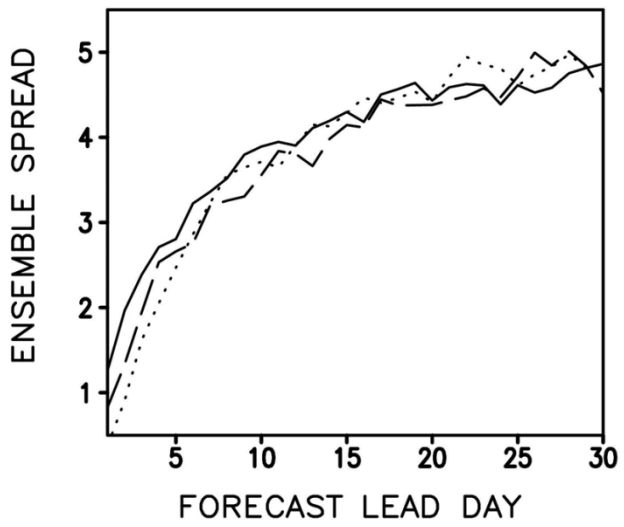

Figure 8. The ensemble spread of 200-hPa zonal wind averaged 15°S-15°N, when the LAF (solid line), the BD (dashed line), and the ESV (dotted line) methods are used.

4.2. Multi-perturbation ensemble prediction system

The positive effect on predictability of breeding and ESV methods is brought from optimal perturbations for intraseasonal oscillation mode. They are generated intentionally in accordance with an ISO-targeted prediction well. This effect becomes apparent when we increase the size of the ensemble members (Table 1).

The multi-perturbation ensemble predictions were made by compositing all eight ensemble members (four members from the LAF prediction, two from the BD, and two from the ESV). Figure 9a shows the correlation skills of the MP ensemble prediction for different time leads along with those of the LAF predictions. The MP ensemble prediction has a higher correlation skill for all time leads compared to those of the LAF predictions. A significance test of the difference between the two correlation skills indicates that the two skills are different with a 95% confidence level. The confidence level is calculated by applying the Student's t-test to six combinations of two members, which were arbitrarily chosen from the four LAF predictions. The skill improvement of the MP prediction was examined for the

strong and weak MJO cases separately. The strong (weak) MJO is classified in terms of the amplitude of the initial RMM index above (below) one standard deviation of the RMM index. As shown in the figure, the skill improvement of the MP predictions is more effective for the weak MJO case (Fig. 9c) compared to the strong MJO case (Fig. 9b). This result is consistent with those of previous studies which showed that predictions using fast growing perturbations improve predictability, particularly in the event of a weak signal (Xue et al. 1997a, b; Cai et al. 2003; Kug et al. 2010).

Figure 10 shows the correlation skill of the MP predictions for eight different initial phases and for different lead times. For lead times of less than 10 days, the prediction skills are similar for the eight phases. After day 15, the prediction skill becomes higher for phases 3 and 8, when large convective anomalies locate in the eastern Indian Ocean, and lower for phase 7 compared to those of the other phases. It was noted that the correlation skill drops to 0.5 by day 17 for phase 7, whereas the correlation skill remains above 0.5 even after day 30 for phase 3. This skill difference indicates that the growth rate of the MJO

depends on the MJO phases.

The RMM index is calculated based on the extended EOF of the three variables. Therefore, this index represents the MJO feature commonly appearing among the three variables, and the regional differences between the prediction skills cannot be assessed with the RMM index. In this case, we examine the spatial distributions of the MP prediction skills of the upper-level wind field and the OLR over the tropical region. The ISO anomaly data used here is obtained by removing the seasonal cycle and the proceeding 120-day mean. Figure 11 shows the spatial distribution of the correlation skill of the 200 hPa zonal wind anomaly for several lead times, and Figure 12 depicts this for those of the OLR. Overall, the correlation skill of the wind field is much better than that of the OLR for the same lead time. For the upper-level wind, the correlation skill exceeds 0.5 with a lead time of five days and 0.3 with a 15-day lead time in most areas of the tropics. In contrast, the OLR correlation skill drops below 0.5 with a five-day lead time in most of the tropics, and there is no meaningful correlation skill appearing in the tropics with a lead time of 15 days. It was also

noted that the correlation skill of the upper-level wind is essentially distributed uniformly over the tropics, whereas the OLR prediction skills are higher in the Indian ocean and the Maritime continent, where the convective signal is relatively large compared to those of other regions.

Lee et al. (2012) investigated the ISO characteristics during the boreal summer and proposed a new ISO index, which better represents the boreal summer ISO over the Indian and western Pacific region compared to the RMM indices. The computation procedure of the boreal summer ISO (BSISO) index is similar to that of the RMM index except for the domain of interest, which is confined to the region of 10°S-40°N and 40°-160° E. It captures both eastward and northward propagating modes over the Asian monsoon region during the summer. Here, it would be interesting to examine the predictability of the BSISO index, as the present study focuses on the boreal summer ISO. The BSISO index of the prediction and the observed counterpart were calculated by following the procedure described in Lee et al. (2012), and its correlation skill was then computed using the MP

ensemble prediction hindcast data, as displayed in Figure 13. Interestingly its prediction skill is much lower than that of the RMM index, although the BSISO better represents the summer ISO. This may stem from the fact that the BSISO represents the regional-scale ISO over the Asian monsoon region, whereas the RMM index represents the planetary-scale ISO over the tropics, which can be better captured by the model.

Table 1. Summary of EOF analysis on the combined daily fields of equatorially-averaged (15°S to 15°N) OLR, 850hPa zonal wind, and 200 hPa zonal wind from different ensemble members for the period of 1989 to 2008 (20 years). The annual cycle and interannual variability were removed in the all analyzed field and then anomalies were normalized by the area-averaged standard deviation over 15 °S – 15 °N.

Ensemble (number of Ensemble member)	**Explained variance of EOF1 and EOF2**
OBS	28.54 %
LAF (4)	25.38 %
BRED and ESV (4)	27.12 %
LAF (6)	26.15 %
LAF, BRED and ESV (6)	28.70 %

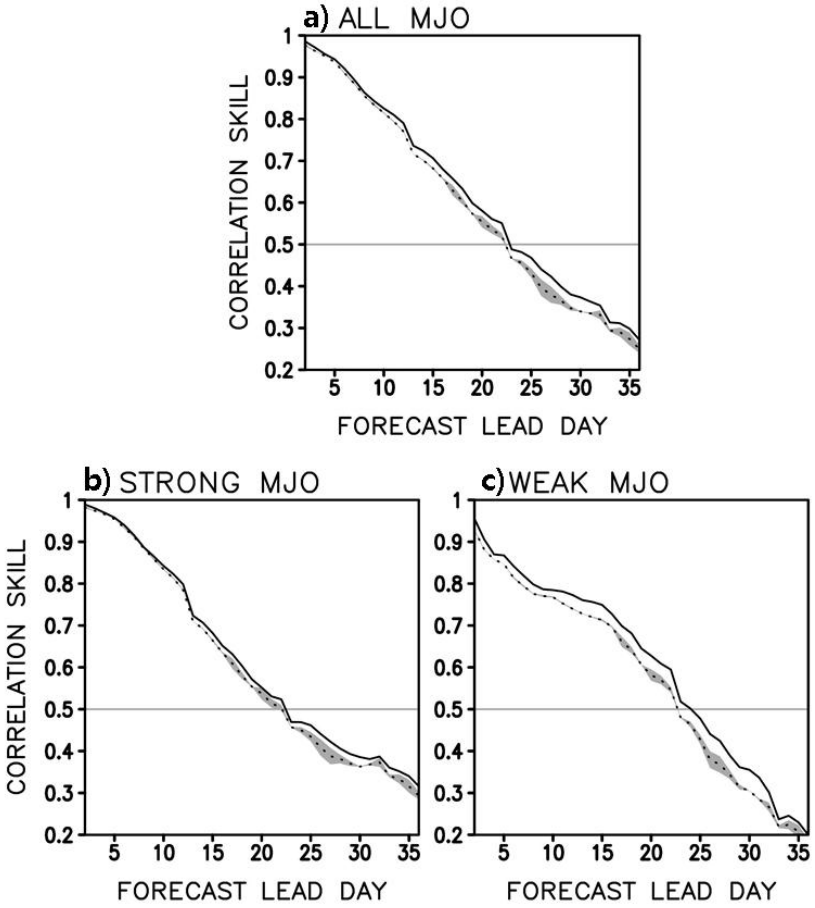

Figure 9. Correlation skill for the RMM index (Wheeler and Hendon, 2004) of the LAF predictions (dotted line), and the MP (solid line) predictions for the a) all, b) strong, and c) weak MJO cases. The strong (weak) MJO case when the initial MJO amplitude, which is defined as the square root of the RMM1 plus RMM2 variance, is larger (smaller) than one.

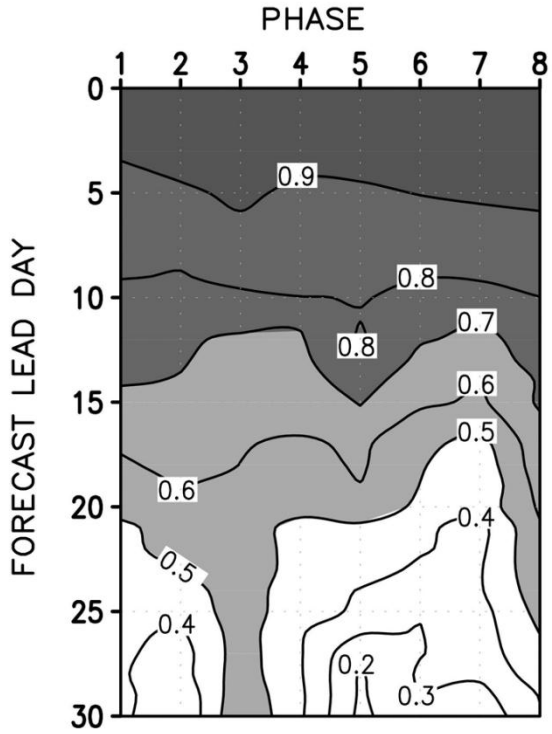

Figure 10. Correlation skill for the RMM index of the MP-based predictions with respect to each initial MJO phases.

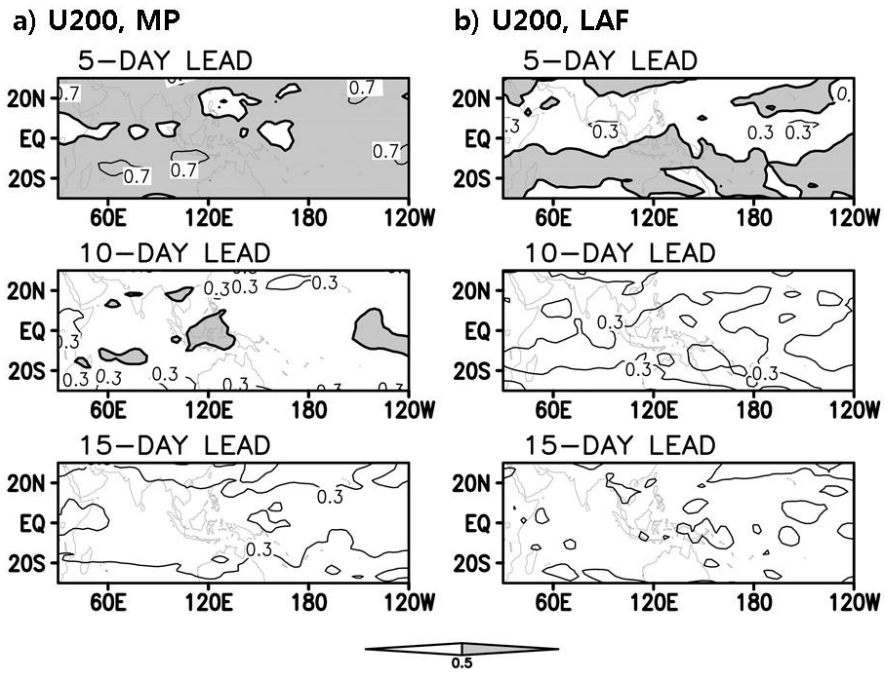

Figure 11. Anomaly correlation coefficients for the 200-hPa zonal wind with interannual variability removed, for a) the MP predictions and b) the LAF predictions as the leading forecast days. Contour interval is 0.2 and the thick contour indicates regions with coefficients as high as 0.5.

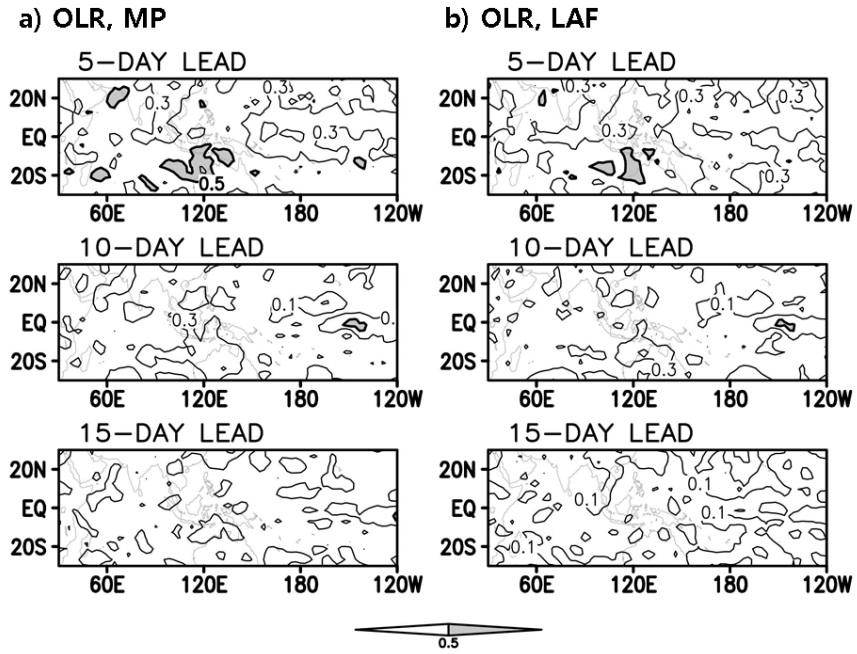

Figure 12. Same as Figure 11, but of OLR with interannual variability removed.

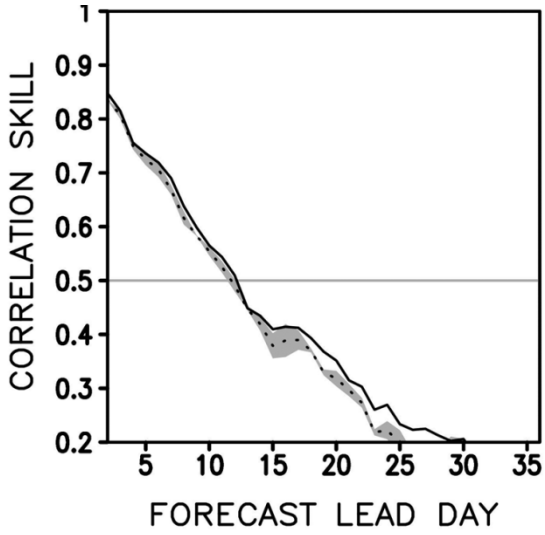

Figure 13. Correlation skill for the BSISO index (Lee et al. 2012) of the LAF predictions (dotted line), and the MP (solid line) predictions for all MJO cases.

5. Summary

In this study, we explored the effect of the initialization and perturbation methods on the ISO prediction system during boreal summer. Three perturbation methods were used, including the LAF, BD, and ESV methods, to perform hindcast experiments. The first two EOF eigenvectors of the LAF perturbations exhibited large variances in the extratropics. The EOF modes of the bred perturbations appeared as quadrature pairs which explain the eastward and northward propagating variabilities from the Indian Ocean to the Western Pacific. On the other hand, the EOF eigenvectors of the ESV perturbations had eastward moving planetary-scale variabilities over the tropics. The ensemble hindcasts with the three kinds of individual perturbation methods produced similar correlation skills, however, the MP-based predictions had a significantly higher correlation skill in predicting the RMM index than those of the individual perturbation methods. The predictability of the intraseasonal oscillation was sensitive to the amplitude of the MJO and to the location of the dominant convection

anomaly at the initial state.

There had been a few attempts to utilize several numbers of coupled initial perturbations in the ensemble prediction system. In this study it seems that the adoption of the individual initialization methods is independent of that of the prediction skill for the boreal summer ISO. However, this study emphasizes the need for an approach to combine several perturbation methods. We developed the MP prediction system for ISO prediction. It helps to maximize the advantage of the perturbation methods for operational ensemble prediction with a finite number of ensemble members. Present study lays the foundation for improving the prediction skill in the initialization research field.

Acknowledgements

This work was supported by the National Research Foundation of Korea (NRF) grant funded by the Korean government (MEST) (NRF-

2009-C1AAA001-2009-0093042). This work was also supported by the Brain Korea 21 Project in 2012.

Reference

Behringer DW, Xue Y (2004) Evaluation of the global ocean data assimilation system at NCEP: the Pacific Ocean In: Eighth symposium on integrated observing and assimilation systems for atmosphere, ocean, land surface. AMS 84th Annual Meeting, Seattle, Washington, January 11–15

Buizza R, Houtekamer PL, Toth Z, Pellerin G, Wei M, Zhu Y (2005) A comparison of the ECMWF, MSC, and NCEP global ensemble prediction systems. Mon Weather Rev 133:1076–1097

Buizza R, Miller M, Palmer TN (1999) Stochastic representation of model uncertainties in the ECMWF Ensemble Prediction System. Q J Roy Meteor Soc 125:1908–2887

Cai M, Kalnay E, Toth Z (2003) Bred vectors of the Zebiak-Cane model and their potential application to ENSO predictions. J Clim 16:40–56

Chikamoto Y, Mukougawa H, Kubota T, Sato H, Ito A, Maeda S (2007) Evidence of growing bred vector associated with the tropical intraseasonal oscillation. Geophys Res Lett 34:L04806 doi:10.1029/2006GL028450

Ding R, Li J, Seo KH (2011) Estimate of the Predictability of Boreal Summer and Winter Intraseasonal Oscillations from Observations. Mon Weather Rev 139:2421–2438

Ding R, Li J, Seo KH (2010) Predictability of the Madden-Julian

oscillation estimated using observational data. Mon Weather Rev 138:1004–1013. doi:10.1175/2009MWR3082.1

Frierson DMW, Kim D, Kang IS, Lee MI, Lin JL (2011) Structure of AGCM-Simulated Convectively Coupled Kelvin Waves and Sensitivity to Convective Parameterization. J Atmos Sci 68:26–45. doi:10.1175/2010JAS3356.1

Ham YG, Kang IS (2010) Growing-error correction of ensemble Kalman filter using empirical singular vectors. Q J Roy Meteor Soc 136:2051–2060. doi:10.1002/qj.711

Ham YG, Schubert SD, Chang Y (2012a) Optimal Initial perturbations for ensemble prediction of the Madden—Julian Oscillation during boreal winter. J Clim 25:4932-4945. doi:10.1175/JCLI-D-11-00344.1.1

Ham YG, Kang IS, Kug JS (2012b) Coupled bred vectors in the tropical Pacific and their application to ENSO prediction. Progr Ocean 105:90–101. doi:10.1016/j.pocean.2012.4.5

Ham YG, Kang IS, Kim D, Kug JS (2012c) El-Niño Southern Oscillation simulated and predicted in SNU coupled GCMs. Clim Dyn 39:383–398. doi:10.1007/s00382-011-1157-3

Hoyos CD, Webster PJ (2007) The role of intraseasonal variability in the nature of Asian monsoon precipitation. J Clim 20:4402–4424. doi:10.1175/JCLI4252.1

Jiang X, Waliser DE, Wheeler MC, Jones C, Lee MI, Schubert SD (2008) Assessing the skill of an all-season statistical forecast model for the Madden–Julian oscillation. Mon Weather Rev 136:1940–1956.

doi:10.1175/2007MWR2305.1

Kang IS and Yoo JH (2006) Examination of multi-model ensemble seasonal prediction methods using a simple climate system. Clim Dyn 26:285–294. doi:10.1007/s00382-005-0074-8

Kang IS, Kim HM (2010) Assessment of MJO predictability for boreal winter with various statistical and dynamical models. J Clim 23:2368–2378. doi:10.1175/2010JCLI3288.1

Kessler WS (2001) EOF representations of the Madden–Julian oscillation and its connection with ENSO. J Clim 14:3055–3061. doi:10.1175/1520-0442(2001)014<3055:EROTMJ>2.0.CO;2

Kim D, Kug JS, Kang IS, Jin FF, Wittenberg AT (2008) Tropical Pacific impacts of convective momentum transport in the SNU coupled GCM. Clim Dyn doi:10.1007/s00382-007-0348-4

Kim D, Sobel AH, and Kang IS (2011) A mechanism denial study on the Madden-Julian Oscillation. J Adv Model Earth Syst 3:M12007. doi:10.1029/2011MS000081

Kim D, Sperber KR, Stern W, Waliser D, Kang IS, Maloney ED, Wang W, Weickmann K, Benedict J, Khairoutdinov M (2009) Application of MJO simulation diagnostics to climate models. J Clim 22:6413–6436. doi:10.1175/2009JCLI3063

Kug JS, Ham YG, Kimoto M, Jin FF, Kang IS (2010) New approach for optimal perturbation method in ensemble climate prediction with empirical singular vector. Clim Dyn 35:331–340. doi:10.1007/s00382-009-0664-y

Kug JS, Ham YG, Lee EJ, Kang IS (2011) Empirical singular vector method for ensemble El Niño-Southern Oscillation prediction with a coupled general circulation model. J Geophys Res 116:C08029. doi:10.1029/2010JC006851

Lee JY, Wang B, Wheeler MC, Fu X, Waliser D, Kang IS (2012) Real-time multivariate indices for the Boreal Summer Intraseasonal Oscillation over the Asian summer monsoon region. Clim Dyn doi:10.1007/s00382-012-1544-4

Lee MI, Kang IS, Kim JK, Mapes BE (2001) Influence of cloud-radiation interaction on simulating tropical intraseasonal oscillation with an atmospheric general circulation model. J Geophys Res 106:14219–14233

Liess S, Waliser DE, Schubert SD (2005) Predictability Studies of the Intraseasonal Oscillation with the ECHAM5 GCM. J Atmos Sci 62:3320–3336

Lin JL, Lee MI, Kim D, Kang IS, Frierson DMW (2008) The impacts of convective parameterization and moisture triggering on AGCM-simulated convectively coupled equatorial waves. J Clim 21:883–909

Lo F, Hendon HH (2000) Empirical prediction of the Madden–Julian Oscillation. Mon Weather Rev 128:2528–2543

Magnusson L, Leutbecher M, Källén E (2008) Comparison between Singular Vectors and Breeding Vectors as Initial Perturbations for the ECMWF Ensemble Prediction System. Mon Weather Rev

136:4092–4104. doi:/10.1175/2008MWR2498.1

Maloney ED, Hartmann DL (2000) Modulation of eastern North Pacific hurricanes by the Madden-Julian oscillation. J Clim 13:1451–1460

Molteni F, Buizza R, Palmer TN, Petroliagis T (1996) The ECMWF ensemble prediction system: methodology and validation. Q J Roy Meteor Soc 122:73–119

Moorthi S, Suarez MJ (1992) Relaxed Arakawa-Schubert: a parametrization of moist convection for general circulation models. Mon Weather Rev 120:978–1002

Pacanowski RC (1996) MOM 2 Version 2.0 (Beta) Documentation User's Guide and Reference Model. GFDL Ocean Technical Report 3.2:329

Palmer TN, Buizza R, Molteni F, Chen YQ, Corti S (1994) Singular vectors and the predictability of weather and climate. Philos Trans R Soc Lond 348:459–475

Palmer TN, Alessandri A, Andersen U, Cantelaube P, Davey M, Délécluse P, Déqué M (2004) Development of a European Multimodel Ensemble System for Seasonal to Interannual Prediction (DEMETER). Bull Amer meteor Soc 85:853–872

Rashid HA, Hendon HH, Wheeler MC, Alves O (2011) Prediction of the Madden-Julian oscillation with the POAMA dynamical prediction system. Clim Dyn 36:649–661. doi:10.1007/s00382-010-0754-x

Seo KH, Schemm JKE, Jones C, Moorthi S (2005) Forecast skill of the

tropical intraseasonal oscillation in the NCEP GFS dynamical extended range forecasts. Clim Dyn doi:10.1007/s00382-005-0035-2

Shukla JM, Anderson J, Baumhefner D, Brankovic C, Chang Y, Kalnay E, Marx L, Palmer TN, Paolino D, Ploshay J, Schubert SD, Straus D, Suarez MJ, Tribbia J (2000) Dynamical seasonal prediction. Bull Amer meteor Soc 81:2593–2606

Shukla JM, Fennessy J (1994) Simulation and predictability of monsoons. Proc the Int. Conf Monsoon Variability and Prediction Tech Rep WCRP-84, WCRP, Geneva, Switzerland, pp567–575

Simmons A, Uppala S, Kobayashi S (2007) ERA-interim: new ECMWF reanalysis products from 1989 onwards. ECMWF Newsletter 110:29–35

Slingo JM, Rowell DP, Sperber KR, Nortley F (1999) On the predictability of the interannual behavior of the Madden–Julian oscillation and its relationship with El Niño. Q J Roy Meteor Soc 125:583–610

Sperber KR and Waliser DE (2008) New Approaches to Understanding, Simulating, and Forecasting the Madden–Julian Oscillation. Bull Amer meteor Soc 89:1917–1920. doi:10.1175/2008BAMS2700.1

Tang Y, Kleeman R, Miller S (2006) ENSO predictability of a fully coupled GCM model using singular vector analysis. J Clim 19:3361–3377

Tokioka T, Yamazaki K, Kitoh A, Ose T (1988) The equatorial 30– 60 day oscillation and the Arakawa–Shubert penetrative cumulus

parameterization. J Meteorol Soc Jpn 66:883–901

Toth Z and Kalnay E (1993) Ensemble forecasting at NMC: The generation of perturbations. Bull Amer meteor Soc 74:2317–2330

Toth Z and Kalnay E (1997) Ensemble forecasting at NCEP and the breeding method. Mon Weather Rev 125:3297–3319

Uppala S, Dee DP, Kobayashi S, Berrisford P, Simmons A (2008) Towards a climate data assimilation system: Status update of ERA Interim. ECMWF Newsletter 115:12–18

Vitart F, Woolnough S, Balmaseda MA, Tompkins AM (2007) Monthly forecast of the Madden–Julian oscillation using a coupled GCM. Mon Weather Rev 135:2700–2715

Waliser DE, Jones C, Schemm JKE, Graham NE (1999) A statistical extended-range tropical forecast model based on the slow evolution of the Madden–Julian oscillation. J Clim 12:1918–1939

Waliser DE, Lau KM, Stern W, Jones C (2003a) Potential predictability of the Madden-Julian oscillation. Bull Amer meteor Soc 84:33–50

Waliser DE, Stern W, Schubert SD, Lau KM (2003b) Dynamic predictability of intraseasonal variability associated with the Asian summer monsoon. Q J Roy Meteor Soc 129:2897–2925

Wang W, Schlesinger ME (1999) The dependence on convection parameterization of the tropical intraseasonal oscillation simulated by the UIUC 11-layer atmospheric GCM. J Clim 12:1423–1457

Webster PJ, Hoyos CD (2004) Prediction of monsoon rainfall and river

discharge on 15–30-day time scales. Bull Amer meteor Soc 85:1745–1765

Wheeler MC, Hendon HH (2004) An all-season real-time multivariate MJO index: development of an index for monitoring and prediction. Mon Weather Rev 132:1917–1932

Wheeler MC, McBride JL (2005) Australian–Indonesian monsoon In: Lau KM, Waliser DE (eds) Intraseasonal variability in the atmosphere-ocean climate system, Praxis, Springer Berlin Heidelberg, pp 125–173

Xue Y, Cane MA, Zebiak SE (1997a) Predictability of a coupled model of ENSO using singular vector analysis. Part I: optimal growth in seasonal background and ENSO cycles.. Mon Weather Rev 125:2043–2056

Xue Y, Cane MA, Zebiak SE (1997b) Predictability of a coupled model of ENSO using singular vector analysis. Part II: optimal growth and forecast skill. Mon Weather Rev 125:2057–2073

Yang SC, Kalnay E, Cai M, Rienecker MM (2008) Bred vectors and tropical pacific forecast errors in the NASA coupled general circulation model. Mon Weather Rev 136:1305–1326

국 문 초 록

북반구 여름철 계절 내 변동의 앙상블 예측에 대한 초기화 과정과 섭동 기법의 영향에 대한 연구가 서울대학교 대기-해양 접합모델을 이용하여 진행되었다. 본 연구에서는 lagged-average forecast (LAF) 기법과 breeding 기법, empirical singular vector (ESV)기법의 세가지 앙상블 섭동기법이 고려되었다.

초기 섭동에 대한 empirical orthogonal function (EOF, 경험 직교함수)의 분석을 통해 초기 섭동은 앙상블 섭동 기법에 따라 특징이 다르게 나타나는 것을 보았다. 6 시간 지연을 이용한 LAF 섭동에서는 중위도에 큰 변동성을 나타내었다. 3 일 간격으로 breeding 하여 얻은 초기 섭동은 인도양에서 서태평양에 걸쳐 국지적으로 동진 및 북진하는 변동성을 나타냈으며, ESV 를 이용한 섭동에서는 적도부근에서 행성 규모로 동진하는 변동성을 보였다. 이러한 세가지 섭동 기법을 이용한 Multi-Perturbation (MP) 기법을 적용하여 Real-time multivariate Madden-Julian Oscillation (RMM) 인덱스에 대한 관측과의 상관계수를 보았다. 각각의 단일 앙상블 섭동 기법에 대한 상관계수는 섭동 기법 별로 서로 유사하게

나타났으나, MP 기법에서는 단일 기법을 사용한 경우보다 예측력이 향상되었다. 예측력은 초기 MJO 의 규모에 민감하게 나타났으며 약한 MJO 의 경우에 예측성이 상대적으로 크게 개선되었다.

주요어:

Multi-Perturbation 앙상블 예측, 앙상블 섭동 기법, 북반구 여름철 계절내 진동, Madden-Julian Oscillation

학생번호 : 2011-20378